small NANO MICRO

Actin networks

DOI: 10.1002/smll.200600565

Biomimetic Models of the Actin Cytoskeleton

Camilla Mohrdieck, Florent Dalmas, Eduard Arzt, Rainer Tharmann, Mireille M. A. E. Claessens, Andreas R. Bausch, Alexander Roth, Erich Sackmann, Christian H. J. Schmitz, Jennifer Curtis, Wouter Roos, Simon Schulz, Kai Uhrig, and Joachim P. Spatz*

***T**he cytoskeleton is a complex polymer network that plays an essential role in the functionality of eukaryotic cells. It endows cells with mechanical stability, adaptability, and motility. To identify and understand the mechanisms underlying this large variety of capabilities and to possibly transfer them to engineered networks makes it necessary to have in vitro and in silico model systems of the cytoskeleton. These models must be realistic representatives of the cellular network and at the same time be controllable and reproducible. Here, an approach to design complementary experimental and numerical model systems of the actin cytoskeleton is presented and some of their properties discussed.*

Keywords:
- cells
- mechanical properties
- microfluidics
- self-assembly
- simulations

[*] Dr. C. Mohrdieck
Department of Metallurgy, University of Stuttgart
Heisenbergstrasse 3, 70569 Stuttgart (Germany)
Fax: (+49) 711-689-3412
E-mail: mohrdieck@mf.mpg.de

Prof. E. Arzt
Max Planck Institute for Metals Research
70569 Stuttgart (Germany) and
University of Stuttgart
Heisenbergstrasse 3, 70569 Stuttgart (Germany)

Dr. F. Dalmas
Institut de Chimie et des Matériaux Paris-Est
(ICMPE) CNRS - UMR 7182
94320 Thiais (France)

R. Tharmann, Dr. M. M. A. E. Claessens, Prof. A. R. Bausch, Prof. E. Sackmann
Department of Physics E22, Technical University of Munich
85748 Garching (Germany)

Dr. A. Roth
Siemens Corporate Technology
81730 Munich (Germany)

Dr. C. H. J. Schmitz, Dr. J. Curtis, S. Schulz, K. Uhrig, Prof. J. P. Spatz
Max Planck Institute for Metals Research
70569 Stuttgart (Germany) and
Department of New Materials and Biosystems
University of Heidelberg
69120 Heidelberg (Germany)

Dr. W. Roos
Division of Physics and Astronomy, Free University of Amsterdam
1081 HV, Amsterdam (The Netherlands)

1. Introduction

Many eukaryotic cells are able to respond, often with great agility, to a large variety of intra- and extracellular stimuli such as chemical agents or mechanical and electrical forces. As a reaction to these stimuli, cells can change their shape and elastic stiffness, sense and generate mechanical forces, proliferate and migrate, for example. This versatile responsiveness is to a large extent due to the highly dynamic internal protein network of eukaryotic cells, the so-called cytoskeleton. It is a complex network consisting of several types of polymer fibers that can form very different structures ranging from crosslinked random networks to highly aligned fibers.

A major constituent of the cytoskeleton is the polymer actin, which plays a dominant role in the mechanical and dynamical behavior of cells. Monomeric actin polymerizes to form negatively charged, helical filaments with a diameter of approximately 8 nm and a length that can vary from less than one micrometer to several tens of micrometers.[1] The persistence length of actin filaments, which is a measure of their bending stiffness, is about 17 μm and is thus of the order of the typical contour length of actin filaments.[2]

Actin filaments form two different types of network in the cytoskeleton: the quasi two-dimensional (2D) actin cortex, and the 3D actin network in the interior of the cell.[3,4] The actin cortex consists of partially crosslinked

actin filaments forming a shell that is locally connected to the internal wall of the cell's plasma membrane and that is several hundreds of nanometers thick. Since the thickness is almost negligible compared to its lateral extension (several micrometers), the cortex can be regarded as a quasi-2D network. The interior network is a seemingly random network of crosslinked actin filaments.[5] If the cell is activated by some internal or external stimulus, this network is often penetrated by bundles that consist of parallel, closely aligned actin filaments.[6] Both networks can be locally remodeled on a time scale of a few seconds in response to a stimulus.

To be able to understand the large responsiveness of cells and their mechanical behavior, it is necessary to understand how they sense, process, and also generate forces. This is not only an interesting biophysical problem but also a technological challenge when it comes to the construction of biomimetic engineered networks. Although much research on cell mechanics has been done,[7,8] a comprehensive and conclusive picture is still lacking.[9] One of the reasons for this is the great complexity of cells or even of subcellular systems. The actin cortex and its coupling to the cell membrane, for example, constitute a very complex system for which quantitative studies are difficult to perform. It is therefore very important, and also challenging, to design realistic in vitro model systems that mimic the cytoskeleton in as many respects as possible but that are at the same time controllable and reproducible. Such bottom-up approaches enable access to a quantitative understanding of cytoskeletal mechanics.[8]

In this work, we present novel techniques to design model systems as well as methods to probe the mechanical behavior. Since the cytoskeleton consists of quasi-2D and 3D regions of actin networks that seemingly differ in structure, in structural transitions (e.g., the formation of bundles) and in their physical properties[10] our efforts focus on the design of complementary model systems that describe the topologically different regions of the cytoskeleton and also allow us to analyze their responses to external stimuli, for example, mechanical forces. We stress that all models presented here are minimalist in the sense that they are still far from reproducing the complex behavior of in vivo actin networks, not to mention the behavior of an entire cell. However, they are controllable and can therefore be made progressively more complex in a systematic fashion. We organize the following sections in three parts. The first describes the development of models of the quasi-2D actin cortex. The second and third parts describe an in vitro model and an in silico model of a 3D actin network, respectively, and their mechanical properties.

2. Results

2.1 In Vitro Models of the 2D Actin Cortex

We present two different techniques that mimic the cellular actin cortex in vitro and that allow for a thorough analysis of the constituent protein network. The first approach employs arrays of micropillars made of polydimethylsiloxane (PDMS) to create a locally grafted actin network that self-assembles on top of the micropillars. This freely suspended network is structurally similar to the actin cortex in a cell. It can be modified in a controlled manner by the addition of chemical agents (e.g., actin crosslinking molecules like filamin or divalent magnesium ions) to observe their effect on the actin network.[11]

In a second approach, we replace the fixed micropillars with microspheres, each of which is held fixed by a single optical trap (OT).[12] Once an actin network has formed on top of the microspheres, the network can subsequently be manipulated and its mechanical properties can be measured by moving the optical traps and using them as force sensors. This optomechanical system is realized using holographic optical tweezers (HOTs), a recent and powerful manipulation tool that allows multiple microscopic objects to be moved independently in a noninvasive way and forces in the range of piconewtons to be measured[13,14]

2.2 Micropillar Arrays

The micropillars have a diameter of 5 μm, a height of 12 μm, and are regularly (for special purposes also irregularly) arranged on the surface of the PDMS substrate. If the distances between the pillars is smaller than the persistence length of actin (17 μm), the filaments are freely suspended on top of the pillars and physisorption to the bottom surface of the substrate is prevented. If the interpillar spacing is larger than 17 μm, however, actin filaments attach to the bottom of the substrate, which prevents the formation of a quasi-2D network (experiments not shown). We therefore chose the pillar spacings to be between 5 and 10 μm.

The pillar tops are functionalized allowing actin filaments to attach to these sites. This pointlike anchorage mimics the local coupling of the cellular actin cortex to the membrane. It results in a self-assembled network, the structure of which is determined by the arrangement of the pillars. An example is shown in Figure 1a, which is the top view of a freely suspended and uncrosslinked actin network on micropillars. Here, actin filaments are stabilized and labeled with phalloidin-tetramethylrhodamin-isothiocyanat (phalloidin-TRITC) for visualization.

To mimic the cellular actin cortex, the network in Figure 1a has to be crosslinked. This can be done either with unspecific crosslinkers such as divalent cations or with specific crosslinkers such as filamin. Since actin is a negatively charged polyelectrolyte with a charge density of 4 e nm^{-1} at physiological conditions, it attracts cations from the buffer solution resulting in a so-called counterion condensation.[15] Fluctuations in the counterion charge density along the polyelectrolyte lead to long-range attractions that can overcome the electrostatic repulsion between equally charged polyelectrolytes.[16] In this way, an unspecific homogeneous crosslinking of actin filaments into bundles of filaments can be established.[17]

In our experiments, we crosslinked actin filaments by adding oxygen scavenger at a concentration of 80 mM Mg^{2+}, which results in a network of actin bundles as seen in Fig-

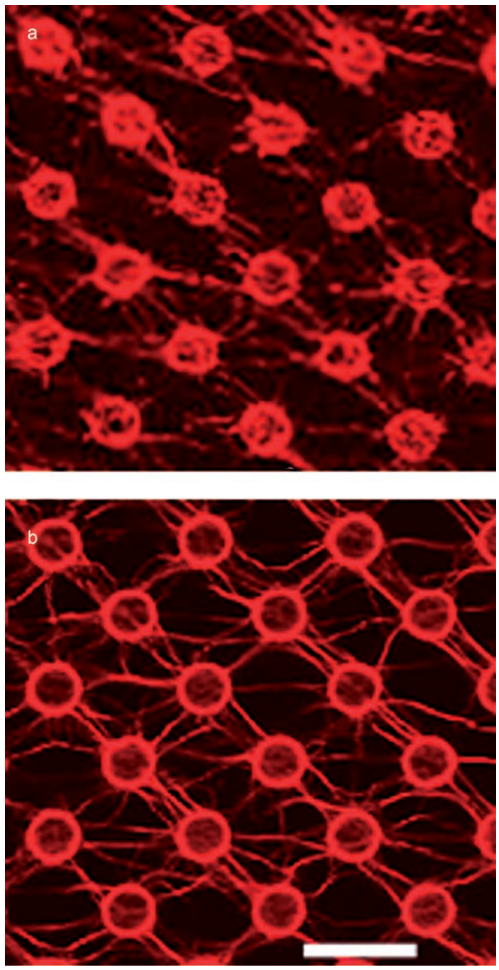

Figure 1. Actin networks on PDMS pillar substrates. a) Uncrosslinked network of single actin filaments. b) After addition of Mg^{2+} ions a quasi-2D network of actin bundles forms. The pictures were imaged with a confocal microscope; the scale bar corresponds to 10 μm.

ure 1b. In this picture, actin bundles correspond to tethers of high fluorescent intensity. Comparison with Figure 1a shows that bundles are much less blurred than the single actin filaments in Figure 1a. This is because filaments undergo large fluctuations in the flow chamber while bundles are much stiffer and hence less subject to fluctuations. Actin bundle formation is not observed if monovalent instead of divalent cations are used as crosslinkers.

A similar network topology can be generated by adding the specific crosslinker filamin, which is a dimeric actin binding protein with a forklike structure that tethers actin filaments in networks and bundles. It leads to the formation of a crosslinked actin network that contains single actin filaments and bundles (not shown).

2.3 Optomechanical Traps

HOTs employ a spatial light modulator to produce multiple optical traps (OTs). An OT comprises a tightly focused laser beam of which the steep electric-field gradients interact with dielectric microparticles such that they are trapped in the focus of the laser beam. The unique capabilities of a HOT apparatus permit the localization of up to hundreds of OTs in a 3D microscopic volume. Individual traps can be moved independently of each other, they can be eliminated, and new traps can be created. To apply this technique to biomimetic actin networks, we integrated HOTs with a new microfluidic platform and a fluorescence microscope to create a powerful and diverse optomechanical microlab that enables a very controlled mechanical and chemical manipulation of the model actin cortex.[18,19]

A demonstration of the flexibility of such a device is given in Figure 2a. Here, microspheres are arranged in arbitrary patterns by moving each sphere individually and independently of its neighbors. Figure 2b and c shows a uniaxial deformation of a regular arrangement of spheres by exerting mechanical forces (arrows) of the order of piconewtons on

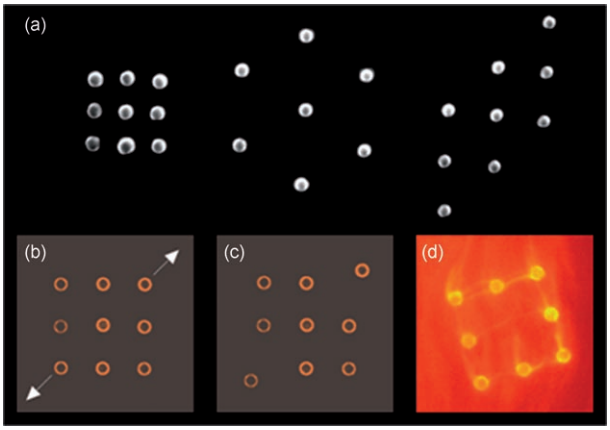

Figure 2. a) Holographic optical tweezers are used to move microspheres (diameter 2 μm) individually and to arrange them in arbitrary patterns. b, c) By applying forces (arrows) of the order of pN, arrangements of microspheres are changed. d) Specific chemical modifications of the surfaces of the microspheres enable the growth of actin networks. The yellow fibers are single actin filaments connecting the spheres that are spatially trapped by holographic optical tweezers.

them. If the surfaces of the microspheres are functionalized to bind actin filaments, this technique principally allows the mechanical activation of actin networks in a very flexible and controlled manner (Figure 2d). The integrated microlab therefore provides the possibility to analyze the viscoelastic properties of a model actin cortex and to tune its chemical complexity by applying a microfluidic chip with multiple channels, enabling a controlled delivery of different chemical solutions to the system.

2.4. In Vitro Model of the 3D Actin Cytoskeleton Crosslinked by Depletion Forces

To study the structural and mechanical properties of the 3D actin cytoskeleton, we constructed 3D in vitro actin networks. The properties of these models depend crucially on the degree to which the networks are crosslinked as well as

on the type of crosslinker. At low concentrations, most crosslinking molecules, such as filamin, result in a structural phase where single filaments are crosslinked isotropically. Above a threshold density of crosslinking points, most crosslinkers result in a composite phase consisting of filaments and bundles of filaments. Purely bundled phases are only induced by a small number of crosslinkers and by depletion forces. These forces originate from small molecules that act as unspecific crosslinkers by inducing purely entropic attractions between the individual filaments.[20] An example of an unspecific crosslinker of small molecules used in in vitro model systems is polyethylene glycol (PEG).[21]

To this date, theoretical models of the mechanical behavior of networks are only capable of describing networks that consist of one structural phase (see Ref. [8] for a review). For this reason, a network crosslinked by depletion forces and containing only bundles of actin filaments is well suited to verify the validity of the theoretical models. In this work, we therefore focus on in vitro 3D actin networks crosslinked by PEG and compare the measured mechanical properties to numerical simulations of deformed actin networks.

We crosslinked in vitro actin networks using depletion forces by adding PEG to solutions of entangled actin filaments and measured the elastic shear modulus G_0. The applied shear strains were small enough ($<10\,\%$) to ensure a linear stress–strain relation. Figure 3 shows G_0 as a function of the concentrations of both PEG and actin. In the mechanical response of the system two regimes can be identified. At low concentrations of PEG, G_0 weakly increases with the PEG concentration; this increase can be described by a power law with an exponent 0.2 ± 0.1 (dashed lines in Figure 3). Above a critical concentration of PEG, c^*, the increase of G_0 with the PEG concentration is much stronger and a power-law fit yields an exponent of 3.5 ± 0.6 for this regime (solid lines in Figure 3). The critical concentration of PEG decreases with the concentration of monomeric actin, c_{actin}, in the solution. It can be calculated numerically if the molecular interactions between the filaments are known.[22–24]

The fit curves in the regime $c_{PEG} < c^*$ have been obtained by assuming that the dependence of G_0 on c_{actin} follows the theoretically predicted scaling law for a crosslinked actin network:[25]

$$G_0 \approx {c_{actin}}^{2.2} \quad (1)$$

For comparison, we also include fit curves in the same concentration regime that are based on the scaling law predicted for entangled actin networks (dotted lines in Figure 3).[26]

At c^* a structural transition is observed; a phase consisting of homogeneously crosslinked actin filaments is found at PEG concentrations below c^*, while a network of homogeneously crosslinked actin bundles is found above c^* (Figure 4a, b). It is important to note, that in the PEG/actin model system no composite phase containing both single filaments *and* bundles simultaneously is observed.

Once the bundles have formed, they increase linearly in diameter with the concentration of PEG. This relation is shown in Figure 4c, where we determined bundle sizes from transmission electron microscopy (TEM) images.

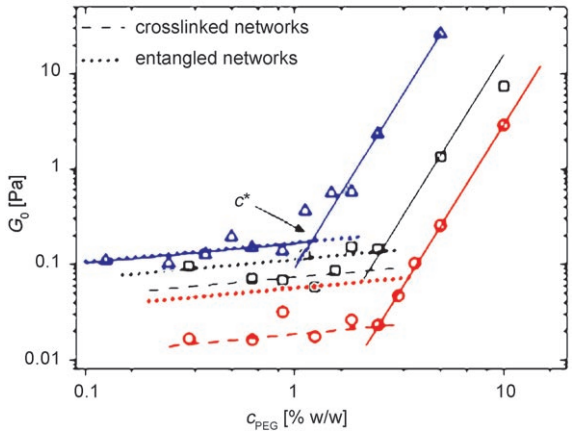

Figure 3. Shear modulus versus concentration of PEG. Two different scaling regimes can be distinguished: $G_0 \approx {c_{PEG}}^{0.2}$ for $c_{PEG} < c^*$ (dashed lines) and $G_0 \approx {c_{PEG}}^{3.5}$ for $c_{PEG} > c^*$ (solid lines). The actin concentrations are 4.75 μM (circles), 9.5 μM (squares), and 14.3 μM (triangles). The value of c^* is indicated (arrow) for a solution with $c_{actin} = 14.3$ μM. In the regime $c_{PEG} < c^*$, the fit curves are obtained by the theoretically predicted scaling law: $G_0 \approx {c_{actin}}^{2.2}$ for crosslinked networks (Equation (1)). For comparison, dotted lines in this regime indicate a fit that assumes that the networks are entangled instead of crosslinked, which clearly does not fit the obtained data.

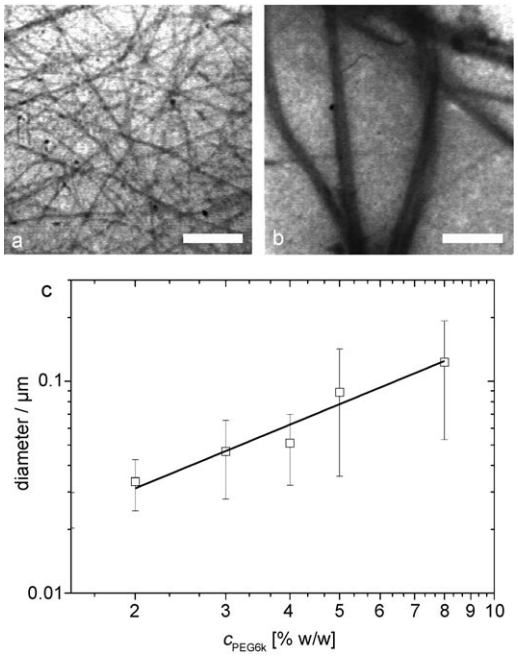

Figure 4. TEM images of actin networks crosslinked with PEG. a) Network of crosslinked actin filaments for concentrations $c_{actin} = 9.5$ μM and $c_{PEG} = 1.5\,\%$ w/w $< c^*$. b) Network of crosslinked actin bundles for $c_{actin} = 9.5$ μM and $c_{PEG} = 8\,\%$ w/w $> c^*$. The scale bars correspond to 0.5 μm. c) Diameter of actin bundles as a function of the concentration of PEG determined by image analysis of TEM images. For $c_{PEG} > c^*$ the diameter increases with c_{PEG}. The concentration of actin is $c_{actin} = 9.5$ μM.

2.5 Numerical Model of the Crosslinked 3D Actin Cytoskeleton

We developed an in silico model of the actin cytoskeleton to complement the in vitro model and to identify the properties of the crosslinker that led to the observations described above. To this end, we model actin filaments as straight fibers of uniform length and diameter. They are randomly distributed and randomly oriented in a confining cubic box that is large enough to ensure that finite-size effects are negligible. All fibers are assigned an elastic modulus corresponding to the value for actin filaments, $E_f = 2$ GPa,[2,27] and a bending stiffness that depends on the chosen aspect ratio of the fibers. Two fibers are 'crosslinked' whenever they touch each other or penetrate each other, which is possible in our model since we do not consider excluded volume effects. The crosslinks are also modeled as short fibers with a uniform diameter and a uniform elastic spring constant K_{link} (Figure 5a). Two different types of crosslink can be defined: 'free links' for which the relative orientation between crosslinked fibers is variable, and 'constrained links' for which this orientation is fixed.

After the fibers have been crosslinked, all dangling fiber ends as well as isolated fibers or clusters of fibers that do not carry any mechanical load are removed. This results in a model system, as shown in Figure 5b, where fibers are presented as black lines and crosslinks between them are presented as grey lines. We deform the model system by applying a homogeneous shear strain along the principal directions (X, Y, Z in Figure 5b) and determine the elastic shear modulus of the system as the average of the moduli for the three directions. This procedure is repeated for a total of ten different but equivalent model systems and the evaluated shear modulus, G_0, is the average of all ten systems. In this way, we can conduct systematic studies of the dependence of G_0 on individual parameters of the crosslinked network.

Figure 6a depicts the dependence of G_0 on the volume fraction ψ of the model actin fibers for the two types of crosslink. Since ψ is proportional to the concentration of the model fibers, this dependence can be directly compared to the measured dependence $G_0 \approx {c_{actin}}^{2.2}$ (dashed lines in Figure 3). To obtain the graphs in Figure 6a we chose a spring constant $K_{link} = 0.1\ \mathrm{N\,m^{-1}}$ in accord with experimentally determined stiffness values for single protein molecules.[28–30] The fiber aspect ratio was chosen to be $\xi = 100$. This value is about a factor of 30 less than the aspect ratio of actin filaments used in the experiments but it constitutes an upper limit of the number of generated fibers that can still be efficiently modeled. The results show that the calculated values of G_0 are about two orders of magnitude larger for constrained links than for free links. However, in both cases are the values within the range of experimentally determined values for in vitro actin networks.[21,25,31–33] Further-

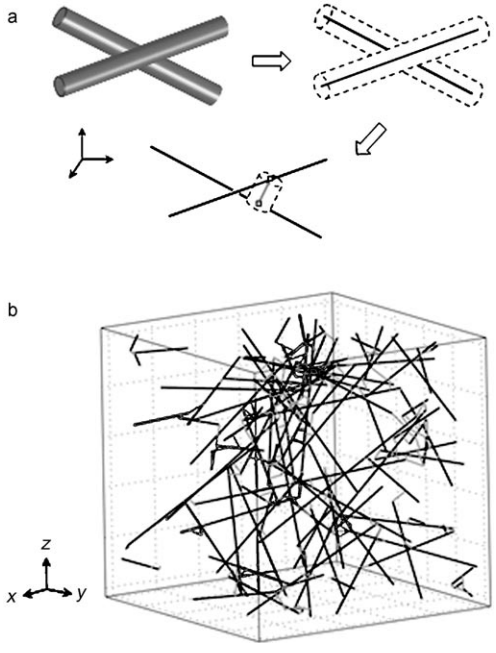

Figure 5. Construction of the numerical model. a) If the distance between the midaxes (solid lines) of two adjacent fibers is smaller than the fiber diameter, a crosslink (small cylinder) is created between the fibers at this site. b) 3D model system consisting of model actin fibers (black lines) and crosslinkers (grey lines) in a confining volume (box).

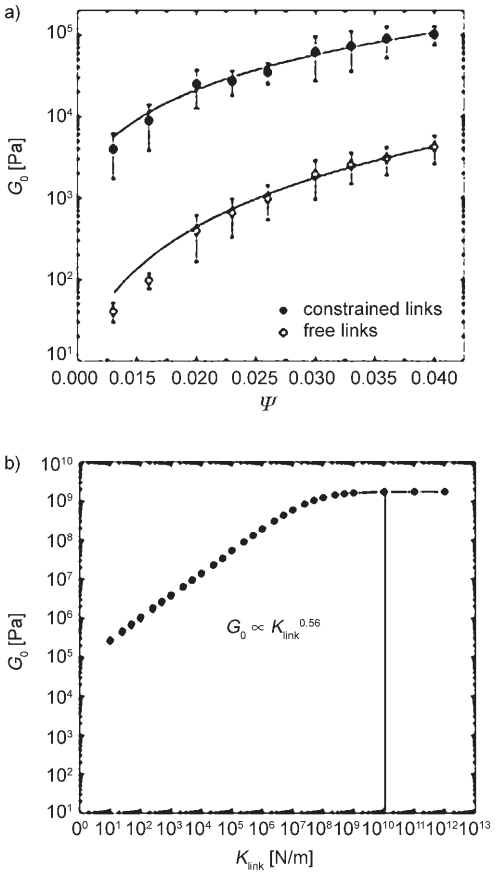

Figure 6. Calculation of G_0. a) Dependence of G_0 on the volume fraction ψ of fibers for constrained and free links and for a fiber aspect ratio $\xi = 100$. b) Dependence of G_0 on the elastic spring constant K_{link} of the crosslinkers for $\psi = 0.04$ and $\xi = 100$ and constrained links. The vertical line marks the spring constant above which G_0 saturates.

more, the fit curves in Figure 6a (solid lines) show that the increase of G_0 with ψ follows different power laws for the two types of link: $G_0 \approx \psi^{2.4}$ for free links and $G_0 \approx \psi^{1.7}$ for constrained links.

To compare our numerical model to the 3D in vitro actin network discussed in the previous section and to further elucidate the effect of c_{PEG} on this network, we calculated the dependence of G_0 on K_{link}. The results are shown in Figure 6b. In these calculations the volume fraction of the fibers was fixed to $\psi = 0.04$ and the fiber aspect ratio was the same as in Figure 6a, while all links were constrained. The increase of G_0 with K_{link} follows a power law with an exponent 0.56 ± 0.002. At $K_{link} = 10^7\,N\,m^{-1}$ (dotted line in Figure 6b) the stiffness of the crosslinkers is the same as that of the fibers. Increasing K_{link} beyond this value leads to a saturation of G_0 because the network is no longer dominated by the stiffness of the crosslinkers but by the fibers making up the network.

3. Discussion

Our studies of 2D actin networks freely suspended on top of arrays of elastic micropillars indicate that such a composite system i) serves as a model to describe the quasi-2D actin cortex and its pointlike anchorage to the cellular membrane and ii) allows forces that are induced in the activated network to be detected.The combination of HOT and microfluidic devices also provides a versatile optomechanical microlab. In this technique, optically trapped microspheres that are connected by actin filaments can act as activators of the network or as force sensors. Both methods are therefore suited to measure the mechanical responses of activated in vitro actin networks, where the HOT technique proves to be especially flexible and precise. In future studies, the complexity of these model systems can be systematically increased to analyze which level of complexity is necessary to mimic a certain property of the actin cortex.

The 3D in vitro actin/PEG model system exhibits a mechanical behavior that is in good agreement with the scaling laws obtained from single-filament models in the concentration regime $c_{PEG} < c^*$ (see dashed lines in Figure 3). This finding indicates that the weak increase of G_0 with c_{PEG} in this regime can be explained by a continuous change from a network dominated by entanglements of filaments to one in which the filaments are crosslinked to one another. This is also supported by our numerical simulations: the power-law dependences in Figure 6a are in good agreement with Equation (1). This is particularly evident for the case of free links, suggesting that crosslinking by depletion forces allows for changes in the relative orientation of the crosslinked filaments as long as the concentration of the depletion agent is small.

As c_{PEG} increases, but is still lower than c^*, the experiments indicate that the unspecific and homogeneous attraction between actin filaments increases and leads to increasingly stronger crosslinks. This is again supported by the simulations that show a power-law increase of G_0 with K_{link} with an exponent 0.56 (Figure 6b) that matches the experimentally measured exponent of 0.2 (dashed lines in Figure 3) well. We also calculated the exponent for free links in the numerical model (data not shown) and found a value of about 0.96. Taken together, the results indicate that i) as c_{PEG} increases, the effective crosslinks mediated by depletion forces progressively suppress orientational changes of the crosslinked filaments; ii) one effect of increasing c_{PEG} is indeed to strengthen the crosslinks elastically.

The experimentally observed strong increase of G_0 for $c_{PEG} > c^*$ and the increasing bundle diameter indicate a continuously increasing homogeneous attraction between the actin filaments, which occurs along the entire lengths of the filaments and therefore renders the formation of bundles and the increase in G_0 very effective. As a matter of fact, applying our simulations to networks of actin bundles (results not shown) revealed that for constant ψ an increase in the number or thickness of bundles alone does not lead to the observed strong increase in G_0. In order to reproduce this increase, it seems to be necessary to also increase K_{link} and hence the strength of the crosslinks, which is exactly what the experiments suggest is happening as c_{PEG} increases.

Our results for the 3D actin model systems imply that depletion forces also contribute significantly to the crosslinking of in vivo actin networks because globular proteins make up 18–27% of the volume of a cell. It is therefore conceivable that depletion forces in cells are strong enough to stabilize the cytoskeleton globally and to alter its structure. Small concentrations of specific crosslinkers could then be sufficient to adjust the network structure locally.

4. Conclusions

The objective of this work is to call attention to the importance of model systems that are able to mimic biological systems, such as the cytoskeleton in eukaryotic cells, that are themselves too complex to be analyzed quantitatively. The development of such a model system involves its design and testing, for example, mechanical testing, to ensure its biomimetic suitability. In this work, we presented novel techniques to design model systems of the quasi-2D actin cortex of cells. We showed that arrays of micropillars can serve as stable supports for freely suspended 2D actin networks. Variations in the geometrical arrangement and elastic stiffness of the pillars can be used to study their influence on the topology of the self-assembling actin network. We also demonstrated that holographic optical tweezers combined with microfluidic devices provide a powerful tool to assemble a network, mechanically activate it, and to study the influence of chemical agents on the network in a controlled manner. Both methods are in the process of being refined to gradually mimic more details of the actin cortex such as the chemical complexity of its focal adhesion sites.[34]

To evaluate the mechanical behavior of 3D in vitro actin networks crosslinked by depletion forces, we measured their elastic shear modulus and compared the results to numerical simulations of sheared actin networks. The results indicate that depletion forces lead to a homogeneously crosslinked

network and that the crosslinks gain in mechanical strength as the concentration of the depletion agent increases, resulting in an increase of the network's shear modulus. This increase has been shown to be particularly large for high concentrations of the depletion agent. In this case, the network is entirely made up of actin bundles. Our quantitative results could help to develop a detailed theoretical explanation of this observation, which is still lacking.

5. Experimental Section

5.1 In Vitro Models of the 2D Actin Cortex

Fabrication of PDMS pillars: The array of PDMS micropillars was fabricated by standard soft lithography techniques as described elsewhere.[35,36] Master fabrication was done by photolithography on a negative photoresist (SU-8 25; MicroChem Corporation) produced by following the protocol provided by the manufacturer.

PDMS is mixed with a thermocrosslinker (curing agent) at a weight ratio of 10:1. Directly after mixing, before it is crosslinked, this mixture is poured onto substrates with cylindrical cavities. By evacuating the air around the substrate and from the holes, the mixture flows into the holes. Curing in an oven results in a flexible PDMS layer exhibiting the micropillars, which can be peeled off the substrate.

Polymerization of actin: Actin and all actin-binding proteins were a generous gift from E. Sackmann and A. Bausch (TU München, Germany). Actin was prepared from rabbit skeletal muscle, as described by Pardee et al.[37] and MacLean-Fletcher et al.[38] and with an additional purification step using gel column chromatography (Sephacryl S-300). Monomeric actin (G-Actin) was polymerized in a polymerization buffer (2 mM trishydroxymethylaminomethane (TRIS), 2 mM $MgCl_2$, 100 mM KCl, 0.2 mM $CaCl_2$, 0.2 mM dithiothreitol (DTT), 0.5 mM adenosine triphosphate (ATP), pH 7.4) for 20 min at room temperature or alternatively for 30 min on ice. The monomer concentration at the start of polymerization was 5 μM (210 $\mu g\,mL^{-1}$). After polymerization the actin was labeled with phalloidin-TRITC (Sigma) in an equimolar ratio of phalloidin-TRITC to G-actin. The actin dilution buffer consists of 25 mM Imidazol, 1 mM ethylene glycol tetraacetic acid (EGTA), 4 mM $MgCl_2$, 25 mM KCl, pH 7.4. As oxygen scavenger, 1 mM DTT, 2.3 $mg\,mL^{-1}$ glucose, 0.1 $mg\,mL^{-1}$ glucose-oxidase and 0.02 $mg\,mL^{-1}$ catalase were added just before use. The water was degassed in an ultrasonic bath for 5 min.

HOT apparatus: The essential component of the HOT technique is the spatial light modulator (SLM), a computer-addressable diffractive optical element of which the liquid crystal display has 512 × 512 liquid-crystal cells (pixels). The HOT beam-splitting element, called a phase mask or hologram, is created on the SLM face where each pixel is assigned one of 130 calibrated phase levels between 0 and 2π. A HOT apparatus with a 512 × 512 reflective SLM (Boulder Nonlinear Systems) imprints the desired phase profile onto the wavefront of a collimated TEM00 laser beam (Spectra-Physics J20-BL-106C, 5 W, $\lambda = 1064$ nm).[18] A 4f telescope adjusts the beam's diameter to perfectly match the back aperture of the microscope objective that focuses the laser light into an optical trap. The telescope also locates the SLM and the high-NA objective (100×, NA = 1.45, oil immersion) in conjugate planes.

5.2 In Vitro Model of the 3D Actin Cytoskeleton Crosslinked by Depletion Forces

Polymerization of actin: Actin was prepared from rabbit skeletal muscle according to Spudich et al. [39] and stored in lyophilized form at −21 °C. For measurements, the lyophilized actin was dissolved in water and dialyzed against fresh G-buffer (2 mM Tris, 0,2 mM ATP, 0,2 mM $CaCl_2$, 0,2 mM DTT , 0.005 % NaN_3) at 4 °C. The G-actin solution was centrifuged at 48 000 rpm and sterile filtrated to minimize the fraction of residual actin-binding proteins. The monomeric actin was kept at 4 °C for a maximum of ten days. Polymerization was initiated by adding 1/10 of the sample volume of 10-fold concentrated F-buffer containing 20 mM Tris (pH 7.5), 2 mM $CaCl_2$, 1 M KCl, 20 mM $MgCl_2$, 2 mM DTT, and 5 mM ATP. Gelsolin was prepared from bovine plasma serum and dissolved and stored in G-buffer at −80 °C. To adjust the mean length of actin filaments to 21 μm gelsolin was added to the sample in the molar ratio of actin to gelsolin $r_{A/G} = 1/7770$ before initiating polymerization. All measurements were done at a temperature of 21 °C. PEG with a molecular weight of 6000 Da (PEG6k) and an approximate radius of gyration of 2 nm (Merck, Germany) was diluted in Millipore water (40 % w/w) and added prior to the polymerization.

Measurement of G_0: The bulk rheological measurements in the linear-response regime were performed with a magnetically driven rotating-disc rheometer. A sample volume of 400 μL was covered with a phospholipid monolayer (dimystriolphosphatidylcholine dissolved in chloroform) to prevent denaturation of actin at the air–water interface. G-actin polymerization was induced by adding 10-fold F-buffer and after 2 min of gentle mixing the polymerizing actin was transferred to the sample cuvette and the lipid layer was spread on the surface. After evaporation of the solvent of the lipids (2 min) the PEG was added with an injection below the lipid film in the sample volume. The rotating disc was placed onto the sample and the cuvette was covered with a glass slide to eliminate any evaporation effects. All rheological experiments were performed after 2 h of polymerization at room temperature. We detected the frequency-dependent moduli $G'(f)$ and $G''(f)$ in a frequency range from $f = 1$ Hz to1 mHz for all samples studied. The elastic shear modulus G_0 corresponds to the plateau modulus at $f = 5$ mHz. The moduli of pure PEG solutions were negligible as they are over the whole frequency regime more than two orders of magnitude below the values measured for the composite actin-PEG networks.

To determine the nonlinear behavior of the networks, the sample was sheared continuously with a constant shear rate of 12.5 % sec^{-1}. These measurements were done with a commercially available rheometer (Physica MCR301, Anton Paar, Graz, Austria). The samples were measured in plate–plate geometry ($r = 25$ mm) with a gap size of 160 μm and a sample volume of 517 μL.

5.3 Numerical Model of the 3D Actin Cytoskeleton

The position of each fiber in the box is defined by five parameters. The first three parameters are the coordinates (x_i, y_i, z) of one extremity of the fiber i and the two other parameters, θ_i and ϕ_i, define the orientation of the fiber. A random and uniform distribution of both the fibers' position and orientation is obtained with (x_i, y_i, z_i), θ_i and ϕ_i varying randomly and uniformly from 0 to the edge length of the box, L_{box}, for (x_i, y_i, z_i), from 0 to 2π for θ_i and from -1 to 1 for $\cos(\phi_i)$.[40] The shear modulus of a given network was obtained from its elastic-strain energy density, which follows from the strain energy of the individual fibers and crosslinks by integration. All simulations were performed using the *Structural Mechanics Module* of the Finite-Element-Programe *Comsol Multiphysics*, version COMSOL 3.2, September 2005.

Acknowledgements

We are grateful to the Volkswagenstiftung for their support of this work. We also gratefully acknowledge the careful preparation of actin and crosslinkers by Junshan Zhang, Michael Bärmann, Monika Rusp, and Hulda Kirpal (TU of Munich), and the synthesis of PEG molecules by Jacques Blümmel (MPI for Metals Research Stuttgart/University of Heidelberg).

[1] M. O. Steinmetz, D. Stoffler, A. Hoenger, A. Bremer, U. Aebi, *J. Struct. Biol.* **1997**, *119*, 295 – 320.
[2] L. Le Goff, O. Hallatschek, E. Frey, F. Amblard, *Phys. Rev. Lett.* **2002**, *89*, 258101.
[3] V. M. Laurent, P. Cañadas, R. Fodil, E. Planus, A. Asnacios, S. Wendling, D. Isabey, *Acta Biotheor.* **2002**, *50*, 331 – 356.
[4] H. Lodish, A. Berk, S. L. Zipursky, P. Matsudaira, D. Baltimore, J. Darnell, *Molecular Cell Biology*, 4th ed., Freeman, Basingstoke, UK, **1999**.
[5] T. M. Svitkina, G. G. Borisy, *Trends Biochem. Sci.* **1999**, *24*, 432 – 436.
[6] M. M. A. E. Claessens, M. Bathe, E. Frey, A. R. Bausch, *Nat. Mater.* **2006**, *5*, 748 – 753.
[7] E. Evans, *Biophys. J.* **1993**, *64*, 1306 – 1322.
[8] A. R. Bausch, K. Kroy, *Nat. Phys.* **2006**, *2*, 231 – 238, and references therein.
[9] D. E. Ingber, *Mech. and Chem. of Biosystems* **2004**, *1*, 53 – 68.
[10] M. Bowick, A. Cacciuto, G. Thorleifsson, A. Travesset, *Phys. Rev. Lett.* **2001**, *87*, 148103.
[11] W. H. Roos, A. Roth, J. Konle, H. Presting, E. Sackmann, J. P. Spatz, *ChemPhysChem* **2003**, *4*, 872 – 877.
[12] A. Ashkin, J. M. Dziedzic, J. Bjorkholm, S. Chu, *Opt. Lett.* **1986**, *11*, 288 – 290.
[13] E. R. Dufresne, G. C. Spalding, M. T. Dearing, S. A. Sheets, D. G. Grier, *Rev. Sci. Instrum.* **2001**, *72*, 1810 – 1816.
[14] J. E. Curtis, B. A. Koss, D. G. Grier, *Opt. Commun.* **2002**, *207*, 169.
[15] J. X. Tang, P. A. Janmey, *J. Biol. Chem.* **1996**, *271*, 8556 – 8563.
[16] G. C. L. Wong, A. Lin, J. X. Tang, Y. Li, P. A. Janmey, C. R. Safinya, *Phys. Rev. Lett.* **2003**, *91*, 018103,1 – 4.
[17] A. Cēbers, Z. Dogic, P. A. Janmey, *Phys. Rev. Lett.* **2006**, *96*, 247801 – 247804.
[18] C. H. J. Schmitz, J. P. Spatz, J. E. Curtis, *Opt. Express* **2005**, *13*, 8678 – 8685.
[19] C. H. J. Schmitz, J. P. Spatz, J. E. Curtis, *Opt. Express* **2006**, *14*, 6604 – 6612.
[20] S. Asakura, F. Oosawa, *J. Chem. Phys.* **1954**, *22*, 1255 – 1256.
[21] R. Tharmann, M. M. A. E. Claessens, A. R. Bausch, *Biophys. J.* **2006**, *90*, 2622 – 2627.
[22] R. de Vries, *Biophys. J.* **2001**, *80*, 1186 – 1194.
[23] A. G. Zilman, S. A. Safran, *Europhys. Lett.* **2003**, *63*, 139 – 145.
[24] M. Hosek, J. X. Tang, *Phys. Rev. E* **2004**, *69*, 051907.
[25] F. C. Mackintosh, J. Käs, P. A. Janmey, *Phys. Rev. Lett.* **1995**, *75*, 4425 – 4428.
[26] B. Hinner, M. Tempel, E. Sackmann, K. Kroy, E. Frey, *Phys. Rev. Lett.* **1998**, *81*, 2614 – 2617.
[27] F. Gittes, B. Mickey, J. Nettleton, J. Howard, *J. Cell Biol.* **1993**, *120*, 923 – 934.
[28] L. Tskhovrebova, J. Trinick, J. A. Sleep, R. M. Simmons, *Nature* **1997**, *387*, 308 – 312.
[29] M. Rief, J. M. Fernandez, H. E. Gaub, *Phys. Rev. Lett.* **1998**, *81*, 4764 – 4767.
[30] M. Yamazaki, S. Furuike, T. Ito, *J. Muscle Res. Cell Motil.* **2002**, *23*, 525 – 534.
[31] M. Tempel, G. Isenberg, E. Sackmann, *Phys. Rev. E* **1996**, *54*, 1802 – 1810.
[32] M. L. Gardel, J. H. Shin, F. C. MacKintosh, L. Mahadevan, P. Matsudaira, D. A. Weitz, *Science* **2004**, *304*, 1301 – 1305.
[33] B. Wagner, R. Tharmann, I. Haase, M. Fischer, A. R. Bausch, *Proc. Natl. Acad. Sci. USA* **2006**, *103*, 13974 – 13978.
[34] E. Zamir, B. Geiger, *J. Cell Sci.* **2001**, *114*, 3577 – 3579.
[35] Y. N. Xia, G. M. Whitesides, *Angew. Chem.* **1998**, *110*, 568 – 594; *Angew. Chem. Int. Ed.* **1998**, *37*, 550 – 575.
[36] D. C. Duffy, J. C. McDonald, O. J. A. Schueller, G. M. Whitesides, *Anal. Chem.* **1998**, *70*, 4974 – 4984.
[37] J. D. Pardee, J. A. Spudich, *Methods Enzymol.* **1982**, *85*, 164 – 181.
[38] S. MacLean-Fletcher, T. D. Pollard, *Biochem. Biophys. Res. Commun.* **1980**, *96*, 18 – 27.
[39] J. A. Spudich, S. Watt, *J. Biol. Chem.* **1971**, *246*, 4866 – 4871.
[40] Z. Néda, R. Florian, Y. Bréchet, *Phys. Rev. E* **1999**, *59*, 3717.

Received: January 11, 2007
Revised: April 4, 2007
Published online on May 8, 2007